SCIENCE CHINA
Chemistry

•ARTICLES•
SPECIAL TOPIC: Precise Catalysis Science and Technology

July 2021 Vol.64 No.7: 1088–1095
https://doi.org/10.1007/s11426-020-9968-x

The selective deposition of Fe species inside ZSM-5 for the oxidation of cyclohexane to cyclohexanone

Liming Zhai[1,2], Bin Zhang[1,2*], Haojie Liang[1,2], Huibin Wu[1,2], Xinchun Yang[1,2], Gen Luo[1,2], Shichao Zhao[1] & Yong Qin[1,2]

[1]*State Key Laboratory of Coal Conversion, Institute of Coal Chemistry, Chinese Academy of Sciences, Taiyuan 030001, China;*
[2]*Center of Materials Science and Optoelectronics Engineering, University of Chinese Academy of Sciences, Beijing 100049, China*

Received November 29, 2020; accepted February 24, 2021; published online March 8, 2021

The design of efficient iron-based catalysts remains a great challenge for selective cyclohexane oxidation to cyclohexanone under mild conditions. Because of the complex distribution of iron location on the support, the selectivity is always low. Here, we report a general strategy to selectively deposit highly-dispersed FeO_x into the micropore of ZSM-5 by atomic layer deposition (ALD). The framework of ZSM-5 and the Brønsted acid sites are intact during ALD, and the Fe species are selectively deposited onto the defect and Lewis acid sites of ZSM-5. Besides, more Fe–O–Si bonds are formed over FeO_x/ZSM-5 with a low loading of Fe, while FeO_x nanoparticles are generated at high Fe loading. They cannot be realized by the traditional solution method. The obtained FeO_x/ZSM-5 catalysts perform high selectivity of cyclohexanone (92%–97%), and ALD cycle numbers of FeO_x control the activity. Compared with the Fe nanoparticles, the Fe–O–Si species performs higher turnover frequency and stability in the oxidation reaction.

atomic layer deposition, selective oxidation of cyclohexane, iron oxide, FeO_x/ZSM-5, Fe–O–Si species

Citation: Zhai L, Zhang B, Liang H, Wu H, Yang X, Luo G, Zhao S, Qin Y. The selective deposition of Fe species inside ZSM-5 for the oxidation of cyclohexane to cyclohexanone. *Sci China Chem*, 2021, 64: 1088–1095, https://doi.org/10.1007/s11426-020-9968-x

1 Introduction

The design of highly-efficient catalysts for selective oxidation of the C–H bond of alkanes at low temperatures is of great importance in both the scientific research and industrial conversion of coal, petroleum, and natural gas [1,2]. For instance, cyclohexane oxidation can produce cyclohexanol and cyclohexanone, which are important intermediate products in the production of nylon-6 and nylon 66 [3–5]. However, the industrial process for the oxidation of cyclohexane by air or oxygen in the presence of homogenous cobalt or manganese salt catalysts suffers from a high reaction temperature and pressure, low activity and selectivity, and severe environmental pollution [1,6,7]. It is highly desirable to develop high-performance heterogeneous catalysts and processes for the oxidation of cyclohexane at low-temperatures.

Compared with other oxidants, such as air, oxygen, and *tert*-butyl hydroperoxide, hydrogen peroxide (H_2O_2) can realize the oxidation of alkanes without producing many by-products, which is expected to realize the selective conversion of cyclohexane at low temperature [8–10]. Many researchers focused on developing a series of supported iron-based catalysts to simulate the alkane biological monooxygenase with iron center atoms [11,12]. In the early days, iron powder, iron-based alloy, iron oxide, and supported iron oxide were used as catalysts for cyclohexane oxidation [13,14]. But the cyclohexanone selectivity is relatively low (<70%), and all the catalysts also suffer from poor stability due to the leaching of iron active sites. After that, many

*Corresponding author (email: zhangbin2009@sxicc.ac.cn)

solvent methods, such as impregnation, ion exchange, and isomorphism substitution, are used to introduce Fe species into the zeolite pores [15,16]. However, it is difficult to control the dispersion and position of iron species. Generally, the Fe ions can easily replace the H^+ of Brønsted acid sites to reduce the number of Brønsted acid sites, and many types of Fe species will be formed on other different potential sites of ZSM-5 (Lewis acid sites and defect sites, *etc*.). The coexistence of multiple active centers on the catalyst became one of the main reasons for the low selectivity.

Atomic layer deposition (ALD) is a thin-film deposition technology by single-layer chemisorption and reaction of vapor precursors on the surface of substrates [17–20]. It can precisely control the size, uniformity, and composition of the metal active species at the atomic or molecular levels by merely changing deposition conditions such as cycle numbers and temperatures [21,22]. Herein, we report a general strategy to selectively deposit high-dispersed Fe species into the micropore of ZSM-5 without the formation of Fe ions by ALD. Ferrocene ($Fe(Cp)_2$) is used as a precursor for the deposition since its kinetic diameter is smaller than the pore size of ZSM-5. Although the ZSM-5 has many potential sites for the deposition in the micropore, the self-limiting reaction between $Fe(Cp)_2$ and the ZSM-5 controls the location of Fe species. The generation of Fe ions is avoided by retaining the Brønsted acid sites. Moreover, the Fe–O–Si bond is selectively formed at low ALD cycles, and Lewis acid sites of ZSM-5 are consumed at high ALD cycles. The obtained FeO_x/ZSM-5 performs a 97% selectivity of cyclohexanone in cyclohexane oxidation, and the turnover frequency (TOF) is controlled by the ALD cycle numbers.

2 Experimental

2.1 Materials

Cyclohexane (99.5%), cyclohexanol (99.5%), cyclohexanone (99.5%), $Fe(Cp)_2$ (99%), tetraethylorthosilicate (TEOS, 99.99%), and tetrapropylammonium hydroxide solution (TPAOH, 50 wt.%) were obtained from Aladdin Chemistry Co. Ltd. Iron(III) nitrate nonahydrate ($Fe(NO_3)_3 \cdot 9H_2O$, 98.5%), acetonitrile (99%) and hydrogen peroxide (30 wt.% in H_2O) were purchased from Sinopharm Chemical Reagent Co. Ltd. ZSM-5 zeolite (SiO_2/Al_2O_3=46) was purchased from Nankai University catalyst Co. Ltd. They were commercial materials of analytical grade and used as received without further purification. Silicalite-1 zeolite was synthesized according to the literature [23].

2.2 Catalyst preparation

Preparation of *m*FeO_x/ZSM-5. ALD process was carried out in a home-made, hot-walled rotation reactor at 270 °C using $Fe(Cp)_2$ and ozone as the precursors. 500 mg of ZSM-5 or silicalite-1 was located in the rotation reactor for each deposition. The size and content of FeO_x in ZSM-5 were controlled by the ALD cycle number (*m*), and the obtained catalyst was denoted as *m*FeO_x/ZSM-5. Ultrahigh purity N_2 (99.999%) was used as a carrier gas at a flow of 70 mL min^{-1}. The $Fe(Cp)_2$ precursor container was heated to 100 °C to obtain sufficient vapor pressure. The pulse, exposure, and purge time for $Fe(Cp)_2$ were 10, 30, and 300 s, and those for ozone 1, 10, and 150 s, respectively. 10FeO_x/silicalite-1 was obtained using the similar method mentioned above.

Preparation of 0.27 wt.%Fe-ZSM-5. The liquid impregnation was used to prepare the catalyst, 38.96 mg $Fe(NO_3)_3 \cdot 9H_2O$, and 2 g ZSM-5 were added into 2 mL deionized water and stirred for 2 h at room temperature. The samples were obtained after the solution was dried at 110 °C overnight and then calcined at 550 °C for 2 h.

2.3 Characterizations

N_2 adsorption-desorption experiments were performed on a Micromeritics ASAP 2020 HD88 system at the standard boiling point of N_2 (−196 °C). Samples were degassed for at least 8 h at 200 °C under a high vacuum before each analysis. Transmission electron microscopy (TEM), high-resolution TEM (HRTEM), scanning transmission electron microscopy (STEM) images, and energy dispersive X-ray spectroscopy (EDX) mapping were taken with a JEOL-2100F field-emission transmission electron microscope operated at 200 kV. The content of Fe in the catalysts was determined by inductively-coupled plasma optical emission spectrometry (ICP-OES, Agilent 725). The X-ray photoelectron spectra (XPS) were collected on a Kratos AXIS ULTRA DLD system with an Al K_α source (1,486.6 eV), and the C 1s peak at 284.8 eV was used as a reference for calibration. X-ray powder diffraction (XRD) analysis was carried out on a Bruker D2 PHASER X-ray powder diffractometer, with Cu K_α radiation (λ=0.154 nm) operated at 40 kV.

Infrared spectra (IR) were recorded at ambient temperature on a Bruker Tensor II IR spectrometer equipped with a liquid-nitrogen-cooled mercury cadmium telluride (MCT) detector at a resolution of 2 cm^{-1}. The nature of the acid sites of the catalysts was determined by pyridine-IR (Py-IR) on a PE Frontier FT-IR instrument with a resolution of 1 cm^{-1}. The samples were dehydrated at 400 °C for 2 h under a vacuum of 10^{-2} Pa, followed by adsorption of purified pyridine vapor at room temperature for 1 h. The system was then degassed and evacuated at different temperatures, and the Py-IR spectra were recorded.

Raman spectroscopic analysis was performed on a Horiba Scientific LabRam HR Evolution microscope with laser excitation wavelengths of 532 nm. An *in-situ* cell was used

to measure the Raman spectra under atmosphere pressure conditions at 20 °C. Powder of the *m*FeO_x/ZSM-5 sample (0.05 g) was pressed into a self-sustaining tablet. Then, 20 μL of H_2O_2 aqueous solution was dropped onto the surface of the tablet. After 5 min, 20 μL of cyclohexane was added to the above system, and the Raman spectra were recorded for each step.

Electron paramagnetic resonance (EPR) spectra were recorded using a Brucker EMX spectrometer (EMXplus-10/12) spectrometer operating at 100 kHz field modulation. Diffuse reflectance ultraviolet-visible (UV-vis) spectra were examined by using a Thermo Scientific Evolution 220 spectrophotometer. For *in-situ* experiments, we obtained the UV-vis spectra of the reaction solvent for different stages.

2.4 Oxidation of cyclohexane

The oxidation of cyclohexane was carried out at 70 °C in a stainless-steel autoclave containing a 50 mL Teflon liner vessel. In each experiment, 0.3 mL cyclohexane was mixed with 10 mL of acetonitrile solvent and 0.20 g of catalyst. Then, 0.48 mL of 30 wt.% aqueous solutions of hydrogen peroxide was added slowly into the mixture. The autoclave was flushed with argon three times and pressurized to 0.4 MPa Ar (99.999%). The reaction mixture was heated to the desired temperature (typically 70 °C) at a stirring speed of 1,000 rpm. At the end of the reaction, the solid particles (catalyst) were separated by filtration, and the products were identified by gas chromatography-mass spectrometry (Agilent Technologies 7890A-5795C) equipped with an FID detector and 30 m HP-5 capillary column. The products were detected by gas chromatography (GC-9720, Zhejiang FuLi chromatogram, China) equipped with an FID detector and a 30 m HP-5 capillary column.

3 Results and Discussion

3.1 Synthesis and characterizations of FeO_x/ZSM-5 by ALD

The *m*FeO_x/ZSM-5 catalyst was prepared by ALD using $Fe(Cp)_2$ and ozone as precursors. A rotating reactor was utilized to enhance precursor diffusion and the collision probability between the support and the precursor. The self-limiting reaction of ALD controls the size and location of Fe species into the micropore of ZSM-5 (Figure 1). First, the $Fe(Cp)_2$ molecules are bonded to the surface sites in the micropore and retain –FeCp fragments to suppress further adsorption. The unreacted $Fe(Cp)_2$ molecules are pumped out through the carrier gas in vacuum. The isolated Fe species are then generated after all the surface cyclopentadiene ligands are oxidized by introducing O_3 gas. The size and the location of FeO_x were further controlled by increasing the ALD cycle number.

The FeO_x/ZSM-5 samples were tested by several technologies. For the 10FeO_x/ZSM-5 catalyst, FeO_x nanoparticles cannot be observed on ZSM-5 zeolites from the TEM and the HRTEM images (Figure 2(a) and Figure S1). Then, STEM and EDX mapping were applied. No nanoparticle can be seen, and Fe species are uniformly dispersed on ZSM-5 (Figure 2(b)). When further increasing the ALD cycle number to 40, several nanoparticles distributed on the surface of ZSM-5 were observed (Figure 2(c)). The N_2 adsorption-desorption results show that the specific surface area, micropore specific surface area, and micropore volume of the FeO_x/ZSM-5 catalyst decrease with the increase of FeO_x ALD cycle numbers compared with ZSM-5 (Table 1 and Figure S2). Therefore, Fe species were mainly deposited into the micropore of ZSM-5. Correspondingly, the Fe content in the *m*FeO_x/ZSM-5 catalyst also increases linearly with the increase of cycle numbers from 0.09 wt.% to 0.29 wt.%, suggesting the self-limiting property of ALD (Figure 3(a)). In the X-ray diffraction (XRD) patterns of the *m*FeO_x/ZSM-5 catalyst (Figure 3(b)), only the ZSM-5 characteristic peaks were observed [24], and no diffraction peak of iron oxide is found. These results indicate that the deposition of highly-dispersed FeO_x into the micropore does not change the lattice structure of ZSM-5.

XPS analysis was utilized to detect the chemical state of FeO_x and its interaction with the ZSM-5 (Figure 4). The Fe 2p peak is deconvoluted into three Fe species, which are ascribed to octahedral Fe (2+, 709.6 eV), octahedral Fe (3+, 711.0 eV), and tetrahedral Fe (3+, 712.9 eV), respectively [25,26], indicating that both Fe(2+) and Fe(3+) species are deposited into ZSM-5. The ratio of Fe(2+) species on 10FeO_x/ZSM-5 is 30%, and the value decreases to 5% on 40FeO_x/ZSM-5. The interaction between Fe species and the ZSM-5 can be revealed from the O 1s, Si 2p, and Al 2p

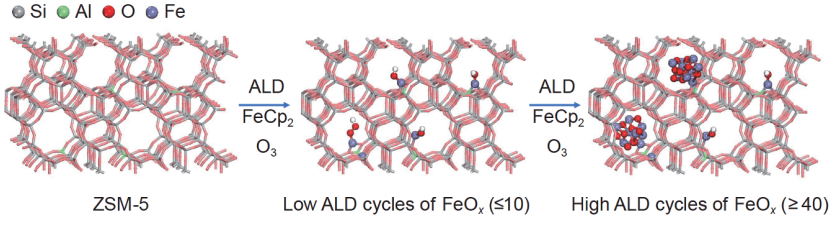

Figure 1 Illustration for deposition of Fe species into the micropores of ZSM-5 (color online).

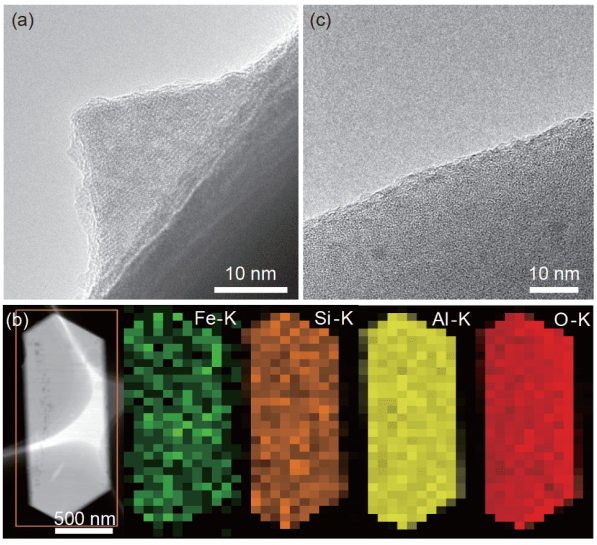

Figure 2 (a) HRTEM image and (b) EDX mapping of 10FeO$_x$/ZSM-5. (c) HRTEM image of 40FeO$_x$/ZSM-5 (color online).

spectra (Figure 4(b–d)). In addition to the Si–O bond of ZSM-5, Both the O 1s (534.06 eV) and Si 2p (104.5 eV) spectra of FeO$_x$/ZSM-5 showed a new peak at high binding energy, indicating the formation of Fe–O–Si bonds [27–29]. The ratio of the Fe–O–Si species over 10FeO$_x$/ZSM-5 is higher than that over 40FeO$_x$/ZSM-5. Moreover, a new peak at 530.1 eV, corresponding to the Fe–O bonds of iron oxide particles, appears in the O 1s spectrum of 40FeO$_x$/ZSM-5. By contrast, the binding energy of the Al–O bond [28] (74.8 eV) does not change with the deposition of the FeO$_x$ cycle number (Figure 4(d)), suggesting no electronic interaction between Fe species and Al oxide species. Therefore, the Fe species selectively bond to the silicon oxide in the form of Fe(2+) at a low ALD cycle number, while iron oxide particles are formed at a high ALD cycle number in the form of Fe(3+).

The interaction between the FeO$_x$ and the acid sites of ZSM-5 was revealed by NH_3 temperature-programmed desorption (NH_3-TPD) (Figure S3) and pyridine adsorption (Figure 5(a, b)). NH_3-TPD measurements show two NH_3 desorption peaks at low and high temperatures, corresponding to weak and strong acid sites [30,31]. The quantification (Table S1) clarifies that both the density of weak and strong acid sites decreases with the increase of Fe loading, indicating the deposition of Fe on acid sites. Pyridine adsorption was used to evaluate the changes for different types of acid sites. Generally, the pyridine adsorption bands at around 1,445 cm^{-1} and 1,545 cm^{-1} are assigned to pyridine coordinated to Brønsted acid sites and Lewis acid sites, respectively [32,33]. The content of acid sites is also calculated (Table S2). The Brønsted acid is dominated over ZSM-5 (0.27 mmol g^{-1} at 200 °C, and 0.19 mmol g^{-1} at 350 °C). Interestingly, the content of Brønsted acid sites at all samples is almost unchanged by increasing the Fe number of ALD cycles. But the number of Lewis acid sites decreases from 0.078 mmol g^{-1} to 0.052 mmol g^{-1} at 200 °C (medium Lewis acid sites) and does not change at 350 °C (strong Lewis acid sites). It is worth noting that the decreasing number of medium Lewis acid sites (7.0×10^{-6} mol g_{cat}^{-1}) is similar to that deposited Fe species (7.7×10^{-6} mol g_{cat}^{-1}) in 10FeO$_x$/ZSM-5. For 40FeO$_x$/ZSM-5, the amount of deposited Fe species (4.0×10^{-5} mol g_{cat}^{-1}) is 1.5 times as high as the re-

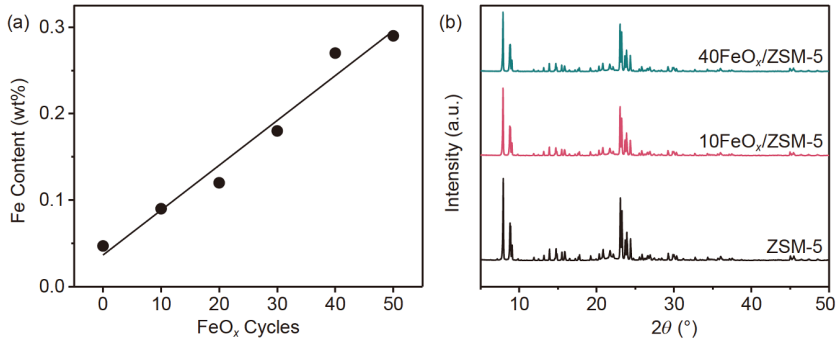

Figure 3 (a) Fe content and (b) XRD patterns of FeO$_x$/ZSM-5 produced with different FeO$_x$ ALD cycle numbers (color online).

Table 1 The physicochemical properties of the samples

Catalyst	S_{BET} (m^2 g^{-1})	S_{micro} (m^2 g^{-1})	S_{meso} (m^2 g^{-1})	V (cm^3 g^{-1})
ZSM-5	369	311	58	0.164
10FeO$_x$/ZSM-5	362	305	57	0.162
20FeO$_x$/ZSM-5	351	295	56	0.157
40FeO$_x$/ZSM-5	349	293	56	0.157

S_{BET}: BET surface area. S_{micro}: *t*-Plot micropore area. S_{meso}: *t*-Plot external surface area. V: BJH pore volume.

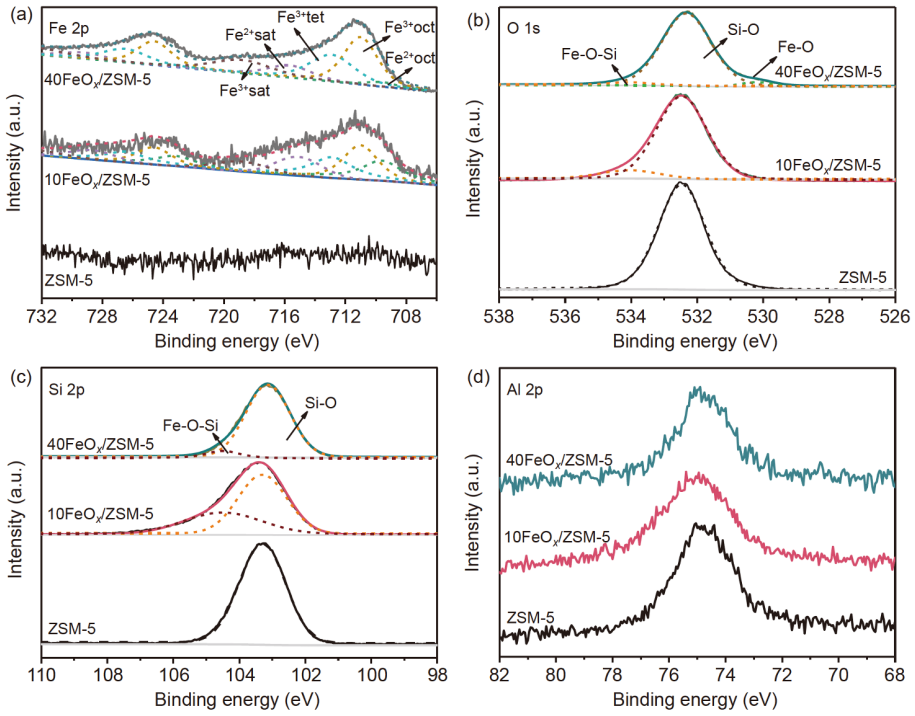

Figure 4 (a) Fe 2p, (b) O 1s, (c) Si 2p and (d) Al 2p XPS spectra from ZSM-5, 10FeO$_x$/ZSM-5 and 40FeO$_x$/ZSM-5 (color online).

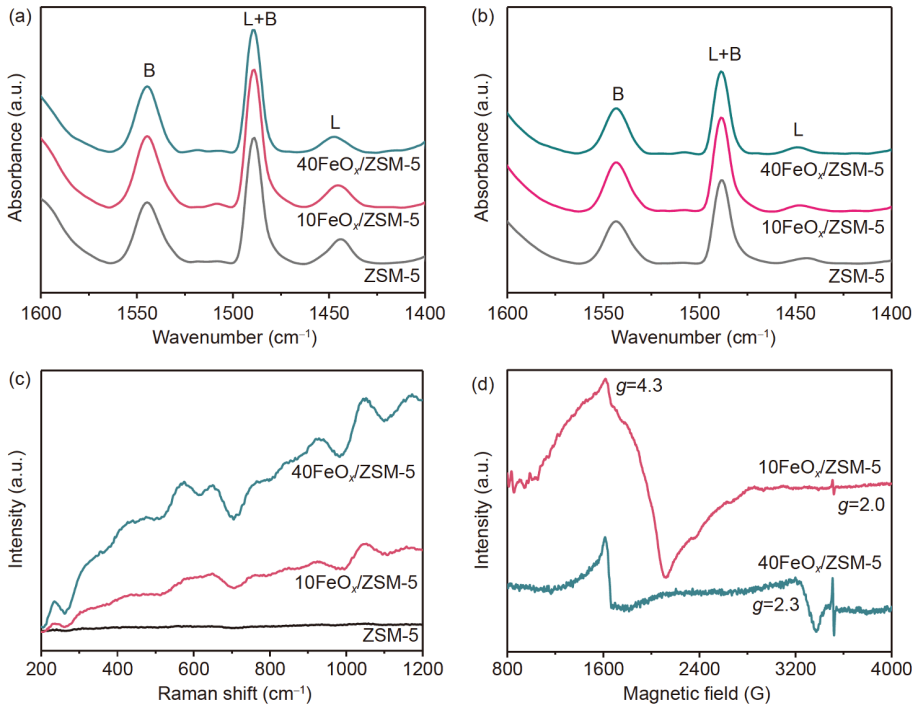

Figure 5 FT-IR spectra of pyridine adsorbed on pure ZSM-5, 10FeO$_x$/ZSM-5 and 40FeO$_x$/ZSM-5 after degassing at (a) 200 °C and (b) 350 °C. (c) Raman spectra (λ_{ex}=532 nm) of ZSM-5, 10FeO$_x$/ZSM-5 and 40FeO$_x$/ZSM-5. (d) EPR spectra of 10FeO$_x$/ZSM-5 and 40FeO$_x$/ZSM-5 at 25 °C (color online).

duced amount of medium Lewis acid sites (2.6×10^{-5} mol g_{cat}^{-1}). Besides, an apparent blue-shift is observed for the adsorption peak on Lewis acid sites. The above results suggest that replacing the H^+ of Brønsted acid sites is suppressed, and Fe species are deposited on the medium Lewis acid sites.

To further reveal the nucleation sites of FeO$_x$ on ZSM-5, EPR and Raman were conducted. The Raman spectra in

Figure 5(c) show many chemical bonds derived from the deposition of FeO_x for $mFeO_x$/ZSM-5. Typical Raman bands at 570 cm^{-1}, 644 cm^{-1}, 1,047 cm^{-1}, and 1,170 cm^{-1} for both $10FeO_x$/ZSM-5 and $40FeO_x$/ZSM-5 can be assigned to the symmetric stretching vibrations of the Fe–O–Si species [34,35], Fe–O stretching mode of Fe(3+)–OOH complexes [36,37], and the Fe–O–Si asymmetric stretching mode of the tetrahedral Fe(3+) in the silica framework [34,36,38], respectively. The EPR signal was also utilized to reveal the chemical bonds of Fe species. In Figure 5(d), Fe species on $10FeO_x$/ZSM-5 exists as two types of isolated Fe species in strong distorted coordination (strong signal, g=4.3) as well as isolated Fe species in high symmetry (weak signal, g=2.0) [39–41]. In addition to the two Fe species in $10FeO_x$/ZSM-5, new trivalent Fe species in the form of superparamagnetic FeO_x particles (g=2.3) are observed for $40FeO_x$/ZSM-5 [42,43].

3.2 The catalytic activity of FeO_x/ZSM-5

Table 2 shows the catalytic performance of ZSM-5 and different FeO_x/ZSM-5 samples in the liquid-phase oxidation of cyclohexane by H_2O_2. Cyclohexanone and cyclohexanol are the two main products. The ZSM-5 has nearly no activity in the oxidation of cyclohexane. The conversion of cyclohexane is enhanced over FeO_x/ZSM-5. A volcanic relationship is observed between catalytic activity and the cycle number of FeO_x, while the selectivity of cyclohexanone increases from 92.5% to 97.3% with the increase of the ALD cycle number. The selectivity of cyclohexanone (>92%) is remarkably high and nearly not changed at different times (Figure 6(a)). The highest conversion is observed over $40FeO_x$/ZSM-5 for a 3.5% conversion of cyclohexane and a cyclohexanone selectivity of 97.1%. The turnover frequency (TOF) is calculated based on the Fe content. It increases with the decrease of the ALD cycle number of FeO_x (m) and reaches the maximum values (5.9 h^{-1}) over $10FeO_x$/ZSM-5. According to the characterization results, more Fe–O–Si species are formed over FeO_x/ZSM-5 with a low loading of Fe, while FeO_x nanoparticles are generated at high Fe loading. The Fe–O–Si species perform the higher intrinsic activity than the FeO_x nanoparticles.

We have also prepared the 0.27 wt.%FeO_x/ZSM-5-IM catalyst with the same Fe loading as $40FeO_x$/ZSM-5 by the

Table 2 Catalyst performances of Fe-based catalysts for the oxidation of cyclohexane

Catalyst	TOF (h^{-1})	Conversion (%)	Selectivity (%)	
			Cyclohexanol	Cyclohexanone
ZSM-5	/	0.4	/	/
$10FeO_x$/ZSM-5	5.9	2.7	7.5	92.5
$20FeO_x$/ZSM-5	4.6	2.8	7.0	93.0
$30FeO_x$/ZSM-5	3.3	3.1	5.4	94.6
$40FeO_x$/ZSM-5	2.6	3.6	2.9	97.1
$50FeO_x$/ZSM-5	2.1	3.2	2.7	97.3
$10FeO_x$/Silicalite-1	3.3	0.6	10.5	89.5
0.27 wt.%FeO_x/ZSM-5	1.6	2.1	15.0	85.0

Reaction condition: 0.2 g catalyst, 0.3 mL cyclohexane, 0.48 mL hydrogen peroxide (30 wt.%), 10 mL acetonitrile, 70 °C, 4 h.

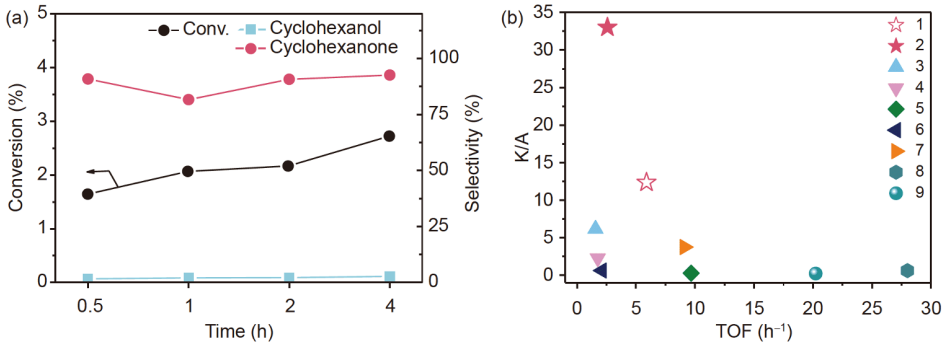

Figure 6 (a) Time-on-line profile for the liquid-phase oxidation of cyclohexane by H_2O_2 over $10FeO_x$/ZSM-5. Reaction conditions: 0.3 mL cyclohexane, 0.48 mL hydrogen peroxide (30 wt.%), 10 mL acetonitrile, 70 °C. (b) Comparison of selectivity and activity with different catalysts for the oxidation of cyclohexane: 1. $10FeO_x$/ZSM-5 (ALD); 2. $40FeO_x$/ZSM-5 (ALD); 3. 0.27 wt.%FeO_x/ZSM-5 prepared by an impregnation method; 4. Fe-ZSM-5 (Impregnation, literature) [8]; 5. Fe-ZSM-5-([emim]BF_4) [8]; 6. Fe-MCM-41 [47]; 7. FeAPO-5 [46]; 8. $FeCl_2$(Tpm) [Tpm=hydrotris(pyrazol-1-yl)methane] [45]. 9. Fe(III)(BPMP)Cl(μ–O)Fe(III)Cl_3 [44]; K: cyclohexanone; A: cyclohexanol (color online).

impregnation method, which performed a low selectivity of cyclohexanone (85%) and also activity. The comparison between FeO_x/ZSM-5 and the reported Fe-based homogeneous and heterogeneous catalysts are shown in Figure 6 (b). The cyclohexanone/cyclohexanol ratio (K/A) over the 10FeO_x/ZSM-5 and 40FeO_x/ZSM-5 reached 12 and 33, which is significantly higher than those reported results over homogeneous catalysts (Fe(III)(BPMP)Cl(μ–O)Fe(III)Cl_3 [44], $FeCl_2$(Tpm) [45], *etc*.), and Fe-based heterogeneous catalysts prepared by the traditional methods (FeAPO-5 [46], Fe-ZSM-5 [8], Fe-ZSM-5([emim]BF_4) [8], Fe-MCM-41 [47]). It is worth noting that all the homogeneous catalysts have shown an extremely low selectivity of cyclohexanone. Thus, the ALD has the advantage of controlling Fe species' location and the selectivity of cyclohexanone.

The reusability of the 10FeO_x/ZSM-5 and 40FeO_x/ZSM-5 was also tested. The selectivity of cyclohexanone decreased after the first use and did not change after further reuse for 10FeO_x/ZSM-5 (Figure 7(a)). For 40FeO_x/ZSM-5 (Figure 7 (b)), the selectivity change is the same as that over 10FeO_x/ZSM-5, while the activity decreased after each reuse. This selectivity decrease might derive from the conversion of Fe species to free Fe ions during the reaction by H_2O_2.

The reusability test results suggest the transform of Fe species during the reaction. *In situ* UV–vis spectra of the catalysts are measured to study the conversion of Fe species during the reaction (Figure 7(c)). Compared with the UV spectrum of H_2O_2 and 10FeO_x/ZSM-5, a new band at 370 cm^{-1} is observed after adding the 10FeO_x/ZSM-5 catalyst and H_2O_2, which can be assigned to the Fe(3+)–OOH complexes [48]. This Fe ion species still exists in the reaction solution when the catalyst is removed by centrifugation. However, no obvious reaction of the filtered solvent (Figure S4) indicates the limited effect of solved Fe species on the cyclohexane oxidation reaction. The *in-situ* Raman spectroscopic analysis was also carried out to further investigate the conversion of Fe species (Figure 7(d, e)). When the H_2O_2 and cyclohexane were sequentially added to the surface of 10FeO_x/ZSM-5, no noticeable change was observed for 10FeO_x/ZSM-5. However, for 40FeO_x/ZSM-5, the intensity of a strong Raman peak at 570 cm^{-1} of Fe–O bonds is significantly decreased and does not recover after adding the cyclohexane. This indicates the irreversible transformation of the FeO_x nanoparticles during the reaction.

To reveal the influence of Brønsted acid sites, we have deposited ten cycles of Fe species on ZSM-5 with different Si/Al molar ratios for cyclohexane oxidation (Table S3). ICP results show that the loading of Fe increases with the decrease of the Si/Al ratio. In general, a low Si/Al ratio means increased Lewis and Brønsted acid sites. However, no positive correlation between the Si/Al ratio and activity (or selectivity) indicates that Brønsted acid sites cannot control the reaction. For catalysts with Si/Al ratios of 13.5 and 23, the loading of Fe is quite similar. But the TOF and activity are lower over 10FeO_x/ZSM-5 with a lower Si/Al ratio (13.5), indicating the negative role of Brønsted acid sites. The Brønsted acid sites and the H_2O_2 solvent provide a solution with strong acidity and oxidization, a harsh environ-

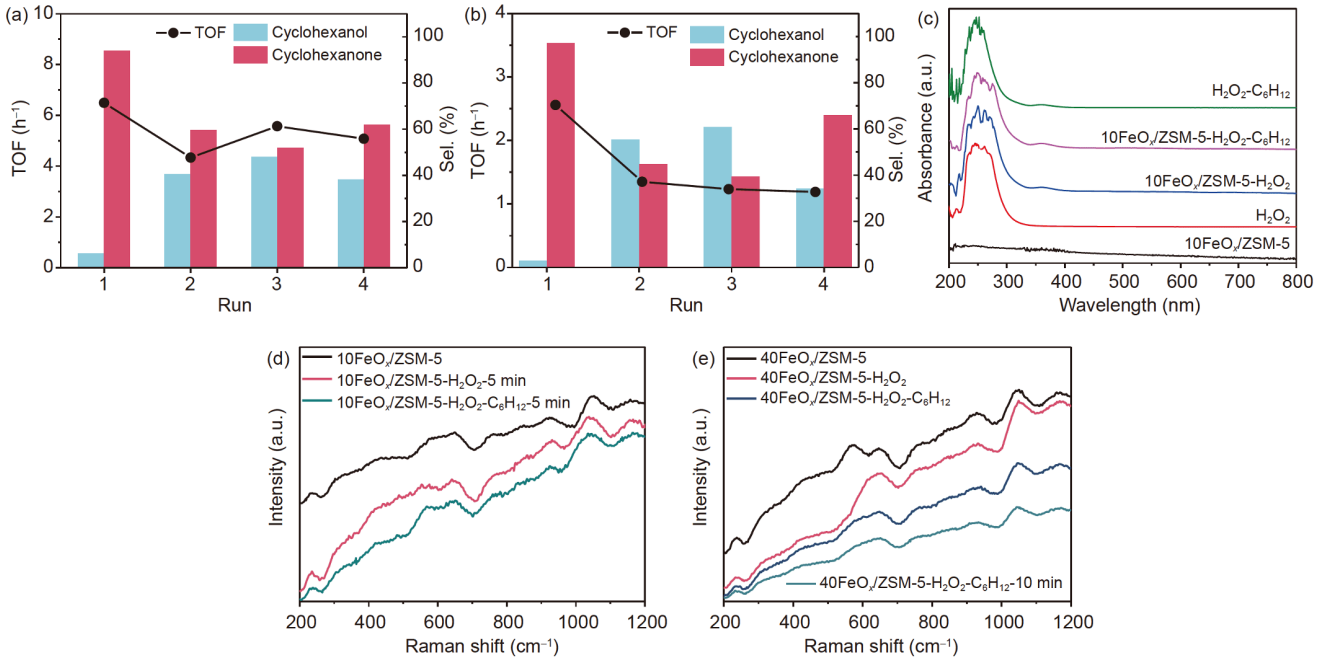

Figure 7 Reusability of (a) 10FeO_x/ZSM-5 and (b) 40FeO_x/ZSM-5. (c) *In situ* UV–vis of H_2O_2 solvent after sequential addition of 10FeO_x/ZSM-5 and cyclohexane. Raman spectra of after sequential addition of H_2O_2 and cyclohexane onto the surface of (d) 10FeO_x/ZSM-5 and (e) 40FeO_x/ZSM-5 (color online).

ment for the Fe species. It expects to bond Fe species on neutral SiO_2 support with strong Fe–O–Si as the right candidate for a highly active, stable oxidation catalyst.

4 Conclusions

In summary, we have successfully synthesized FeO_x/ZSM-5 with only FeO_x (isolated Fe species or FeO_x nanoparticles) by ALD. The formation of free Fe ions is suppressed. The FeO_x/ZSM-5 catalysts perform high selectivity (>92%) of cyclohexanone and TOF in cyclohexane oxidation by H_2O_2. Unlike traditional methods, the Fe species are selectively deposited onto the vacancy sites of ZSM-5 at low ALD cycles and Lewis acid sites at high ALD cycles, respectively. The framework of ZSM-5 and the Brønsted acid sites are intact, and no Fe ions are formed after the deposition. Compared to the FeO_x nanoparticles, the isolated Fe species are bonding with Si in the form of Fe–O–Si, which shows high TOF and stability in the selective oxidation of cyclohexane. The selective deposition of metal oxides into the microporous zeolites by ALD will become a new concept for designing highly-efficient catalysts.

Acknowledgements This work was supported by the National Natural Science Foundation of China (21872160, U1832208), the National Science Fund for Distinguished Young Scholars (21825204), the National Key R&D Program of China (2017YFA0700101 and 2018YFB1501602), the Youth Innovation Promotion Association CAS (2017204), and Natural Science Foundation of Shanxi Province (201901D211591).

Conflict of interest The authors declare no conflict of interest.

Supporting information The supporting information is available online at http://chem.scichina.com and http://link.springer.com/journal/11426. The supporting materials are published as submitted, without typesetting or editing. The responsibility for scientific accuracy and content remains entirely with the authors.

1 Lee S, Halder A, Ferguson GA, Seifert S, Winans RE, Teschner D, Schlögl R, Papaefthimiou V, Greeley J, Curtiss LA, Vajda S. *Nat Commun*, 2019, 10: 954
2 Yang B, Fu Z, Su A, She J, Chen M, Tang S, Hu W, Zhang C, Liu Y. *Appl Catal B-Environ*, 2019, 242: 249–257
3 Shylesh S, Samuel PP, Singh AP. *Appl Catal A-General*, 2007, 318: 128–136
4 Huang X, Zhao G, Wang P, Zheng H, Dong W, Wang G. *ChemCatChem*, 2018, 10: 1406–1413
5 Wan S, Li M, Zhang Z, Xi H, Yang H, Luo Q, Zhu WH. *Sci China Chem*, 2020, 63: 1191–1197
6 Xue K, Yang B, Wu P. *Sci China Chem*, 2015, 58: 139–147
7 Shahzeydi A, Ghiaci M, Farrokhpour H, Shahvar A, Sun M, Saraji M. *Chem Eng J*, 2019, 370: 1310–1321
8 Wang JY, Zhao FY, Liu RJ, Hu YQ. *J Mol Catal A-Chem*, 2008, 279: 153–158
9 Hao J, Wang J, Wang Q, Yu Y, Cai S, Zhao F. *Appl Catal A-General*, 2009, 368: 29–34
10 Acharyya SS, Ghosh S, Bal R. *Green Chem*, 2015, 17: 3490–3499
11 Sirajuddin S, Rosenzweig AC. *Biochemistry*, 2015, 54: 2283–2294
12 Wang VCC, Maji S, Chen PPY, Lee HK, Yu SSF, Chan SI. *Chem Rev*, 2017, 117: 8574–8621
13 Murahashi S, Oda Y, Naota T. *J Am Chem Soc*, 1992, 114: 7913–7914
14 Sun CL, Li BJ, Shi ZJ. *Chem Rev*, 2011, 111: 1293–1314
15 Van-Dúnem V, Carvalho AP, Martins LMDRS, Martins A. *ChemCatChem*, 2018, 10: 4058–4066
16 Graça I, Chadwick D. *Microporous Mesoporous Mater*, 2020, 294: 109873
17 George SM. *Chem Rev*, 2010, 110: 111–131
18 Ge H, Zhang B, Gu X, Liang H, Yang H, Gao Z, Wang J, Qin Y. *Angew Chem Int Ed*, 2016, 55: 7081–7085
19 Zhang B, Qin Y. *ACS Catal*, 2018, 8: 10064–10081
20 Wu H, Zhang B, Liang H, Zhai L, Wang G, Qin Y. *The Innovation*, 2020, 1: 100029
21 Zhang B, Guo XW, Liang H, Ge H, Gu X, Chen S, Yang H, Qin Y. *ACS Catal*, 2016, 6: 6560–6566
22 Liang H, Zhang B, Ge H, Gu X, Zhang S, Qin Y. *ACS Catal*, 2017, 7: 6567–6572
23 Wang N, Sun Q, Bai R, Li X, Guo G, Yu J. *J Am Chem Soc*, 2016, 138: 7484–7487
24 Iliopoulou EF, Stefanidis SD, Kalogiannis KG, Delimitis A, Lappas AA, Triantafyllidis KS. *Appl Catal B-Environ*, 2012, 127: 281–290
25 Yamashita T, Hayes P. *Appl Surf Sci*, 2008, 254: 2441–2449
26 Tan P. *J Catal*, 2016, 338: 21–29
27 Rostamizadeh M, Yaripour F. *Fuel*, 2016, 181: 537–546
28 Zhao Y, Yuan B, Zheng Z, Hao R. *J Hazard Mater*, 2019, 362: 266–274
29 Yan Y, Jiang S, Zhang H, Zhang X. *Chem Eng J*, 2015, 259: 243–251
30 Gu X, Zhang B, Liang H, Ge H, Yang H, Qin Y. *J Fuel Chem Tech*, 2017, 45: 714–722
31 Long Y, Liu S, Fei Y, Li Q, Deng Y. *Sci China Chem*, 2017, 60: 964–969
32 Lin Q, Li J, Ma L, Hao J. *Catal Today*, 2010, 151: 251–256
33 Zhang T, Liu J, Wang D, Zhao Z, Wei Y, Cheng K, Jiang G, Duan A. *Appl Catal B-Environ*, 2014, 148-149: 520–531
34 Li C. *J Catal*, 2003, 216: 203–212
35 Sun K, Fan F, Xia H, Feng Z, Li WX, Li C. *J Phys Chem C*, 2008, 112: 16036–16041
36 Hammond C, Hermans I, Dimitratos N. *ChemCatChem*, 2015, 7: 434–440
37 Chen J, Draksharapu A, Angelone D, Unjaroen D, Padamati SK, Hage R, Swart M, Duboc C, Browne WR. *ACS Catal*, 2018, 8: 9665–9674
38 Wang X, Zhang Q, Yang S, Wang Y. *J Phys Chem B*, 2005, 109: 23500–23508
39 Zhilinskaya EA, Delahay G, Mauvezin M, Coq B, Aboukaïs A. *Langmuir*, 2003, 19: 3596–3602
40 Berrier E, Ovsitser O, Kondratenko E, Schwidder M, Grunert W, Bruckner A. *J Catal*, 2007, 249: 67–78
41 Rana BS, Singh B, Kumar R, Verma D, Bhunia MK, Bhaumik A, Sinha AK. *J Mater Chem*, 2010, 20: 8575
42 Pérez Vélez R, Ellmers I, Huang H, Bentrup U, Schünemann V, Grünert W, Brückner A. *J Catal*, 2014, 316: 103–111
43 Gao F, Zheng Y, Kukkadapu RK, Wang Y, Walter ED, Schwenzer B, Szanyi J, Peden CHF. *ACS Catal*, 2016, 6: 2939–2954
44 Esmelindro MC, Oestreicher EG, Márquez-Alvarez H, Dariva C, Egues SMS, Fernandes C, Bortoluzzi AJ, Drago V, Antunes OAC. *J InOrg Biochem*, 2005, 99: 2054–2061
45 Ribeiro APC, Martins LMDRS, Kuznetsov ML, Pombeiro AJL. *Organometallics*, 2016, 36: 192–198
46 Zhou L, Xu J, Chen C, Wang F, Li X. *J Porous Mater*, 2006, 15: 7–12
47 Wang Y, Zhu J, Li C, Li C, Chen L, Chen M, Wang J. *Appl Chem Ind*, 2009, 38: 1427–1430
48 Bilis G, Christoforidis KC, Deligiannakis Y, Louloudi M. *Catal Today*, 2010, 157: 101–106